Modeling the dynamics of cell-sheet : From Fisher-KPP equation to bio-mechano-chemical systems.

Boutheina Yahyaoui, Mekki Ayadi, Abderahmane Habbal

Modeling the dynamics of cell-sheet : From Fisher-KPP equation to bio-mechano-chemical systems

Fisher-KPP equation to study some predictions on the injured cell sheet

Boutheina Yahyaoui [1] — Mekki Ayadi [2] — Abderahmane Habbal [3]

[1] Tunis El Manar University, National Engineering School of Tunis
ENIT-LAMSIN BP 37, 1002 Tunis, LR 95–ES–20
Tunisia
boutheinayahyaoui@hotmail.fr
[2] Sousse University, Higher School of Sciences and Technology of Hammam Sousse
Street Lamine Abassi, Hammam Sousse 4011
mekki.ayadi@enis.rnu.tn
[3] INRIA, 2004 route des lucioles-BP 93
06902 Sophia Antipolis Nice cedex
France
Abderrahmane.HABBAL@unice.fr

RÉSUMÉ. Dans le cadre de la cicatrisation d'un feuillet cellulaire blessé, nous avons étudié la validité des modèles de réaction-diffusion de type Fisher-KPP pour la simulation de la migration de feuillets cellulaires. Afin d'étudier la validité de ce modèle, nous avons effectué des observations expérimentales sur les monocouches de cellules MDCK. Les videoscopies obtenues permettent, après segmentation et binarisation, d'obtenir avec précision les variations d'aire et de profils de fronts de cicatrice. Nous nous sommes intéressés à comparer les variations des fronts calculés à celles des fronts expérimentaux, après une étape de calage des paramètres.

ABSTRACT. This paper is devoted to study some predictions on injured cell-sheet based on reaction-diffusion equations. In the context of wound cell-sheet healing, we investigated the validity of the reaction-diffusion model of Fisher-KPP type for simulation of cell-sheet migration. In order to study the validity of this model, we performed experimental observations on the MDCK cell monolayers. The obtained videoscopies allow to obtain, after segmentation and binarization, the variations of area and of scar fronts profiles with good accuracy. We were interested in comparing the calculated variations of fronts to those experimental fronts, after a step of calibration parameters.

MOTS-CLÉS : Cellules MDCK, Fisher-KPP, simulation 2D, dynamique cellulaire, coefficient de diffusion D, taux de prolifération r.

KEYWORDS : MDCK, Fisher-KPP, wound edge dynamics, diffusion coefficient D, proliferation rate r, activation, inhibition.

1. Introduction

Medicine and mathematics may seem a bold rapprochement. And yet ... medical imaging provides an unique way to access the inaccessible. Thanks to medical images, physicians and surgeons can see what remains invisible, during an examination, with the naked eye. What is also invisible, it is the essential role of mathematics and computing not only in the formation of these images, but also in their use.

The first decade of the XXIst century witnessed an explosion of works and mathematical articles related to cell dynamics. Living cells obey by nature to complex dynamical processes at the level sub-molecular, molecular, organic, unicellular and multicellular. We are interested in studying the dynamic characteristics of epithelial cell-sheets, using different physical and mathematical fields, to solve any biological phenomena that are difficult to solve.

Modeling cell dynamics is very important issue and at the intersection of three major science fields, biology for the part of experimental measurement and filtering data, mechanical for modeling the tissue movement, mathematical and numerical modeling to quantify biological and mechanical quantities previously mentioned. A large explosion of research is related to cell dynamics and its important role for the resolution of a complex biological problems. We can take as exemple the interested publishement of J.D. Murray describing the relationship between biology and mathematics [1, 2], where he proposed a vision of a mathematician to study reaction-diffusion models that describe the problem of interaction between biological, chemical and mechanical phenomena.

Modeling mechano-chemical behavior coupled with a complex biological systems, such as the formation of an embryon, tumor growth and wound healing, is in mathematical term won by partial differential equations of reaction-diffusion type [3]. This family of equations is well suited to describe in time and in space changes that occur within the production of the migration and the proliferation of cell population. Roughly, the cell diffusion is related to their roving, while the reaction is related to their proliferation. Reaction-diffusion equations coupled to mechanics, with viscoelastic behavior, take into account haptotaxis and haptokinesis phenomenas of cell movement [4].

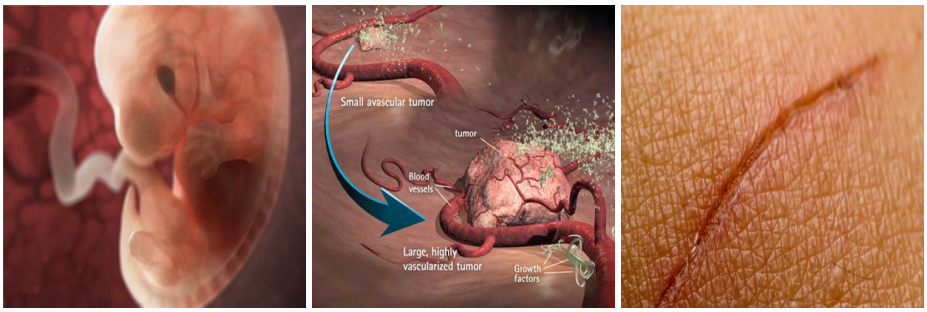

Figure 1. *Formation of a pattern in embryogenesis, tumor growth and wound healing, http ://www.linternaute.com/science/biologie/dossiers/07/cerveau-sexe/page4.jpg, http ://www.santevitalite.be/wp-content/uploads/2012/12/Croissance-tumorale.jpg, https ://www.simplyscience.ch/system/html/Croute-01b7ea33.jpg*

Embryogenesis, tumoral growth and wound healing implies a complex movement of epithelial cell sheet. Moreover, a large percentage of tumors in adult mammals found in epithelial tissue. Development and aggressiveness of cancer is closely related to the cell migration and the cell proliferation occur in epithelial cell lines. These both mechanisms are the most important during the resolution of the biological processes. Cancer cells that produce from epithelial tissues lose epithelial specific cell-cell junctions, but these transformed cells are not destitute of cell-cell adhesion proteins.

In this study, we focus on a particular aspect of wound healing, namely that relative to the flow of monolayers of wounded epithelial cells of Madin-Darby Canine Kidney (MDCK) [5, 6]. The cell population in epithelial monolayer, also called cellular sheet can be considered a two-dimensional structure. After creating a wound, the cells begin to move in order to fill the empty space. Although wound closure involves biochemical and biomechanical process, still far from being understood, which are distributed throughout the monolayer, particular attention was paid to changes in the front. Moreover, the effects of migration activators of HGF (Hepatocyte Growth Factors) type [7] and the effects of inhibitors of PI3K (phosphoinositide 3-kinase) type were taken into account in an experimental test campaign.

Maini, Olsen and Sheratt, in [4], [8], [9], are presented a complete coupled model whose basic variables are cell densitie n, the densitie of ECM ρ and the displacement of tissue u, see the following equations.

$$\frac{\partial n}{\partial t} + div[n\frac{\partial u}{\partial t} + \chi(\rho)n\nabla\rho - D(\rho)\nabla n] = rn(1-n), \tag{1.1}$$

$$\frac{\partial \rho}{\partial t} + div[\rho\frac{\partial u}{\partial t}] = \varepsilon n(1-\rho), \tag{1.2}$$

$$div(\sigma) = \rho s u, \tag{1.3}$$

where

• $div(n\frac{\partial u}{\partial t})$ represents the passive convection, while, $div(\chi(\rho)n\nabla\rho)$ represents the haptotaxis phenomenon, $(-div(D(\rho)\nabla n)$ represents the haptokinesis phenomenon and $rn(1-n)$ represents the cell proliferation,

• $div(\rho\frac{\partial u}{\partial t})$ represents the passive convection, while $\varepsilon n(1-\rho)$ represents the ECM biosynthesis and the degradation of cells fibroplast,

• $\sigma = \sigma_{ECM} + \sigma_{cell}$ with $\sigma_{ECM} = \mu_1\frac{\partial \varepsilon}{\partial t} + \mu_2\frac{\partial \Theta}{\partial t}I + \frac{E}{1+\nu}(\varepsilon(u) + \frac{\nu}{1-2\nu}\Theta I)$ represents the viscous and elastic forces, while, $\sigma_{cell} = cnI$ represents the traction forces, $\varepsilon(u) = \frac{1}{2}(\nabla u + \nabla u^T)$ is the strain tensor and $\Theta = tr(\varepsilon)$ is the dilatation of the matrix material.

Many scientific articles describe in detail the coupled model $(1.1) - (1.3)$. These include for example that of Perelson and *all*, [10], in this paper, it is shown how the above equations are found as well as their numerical implementation. In [11], Sherratt offered monodimensionel and another bidimensional model which include only biomechanical coupling to describe cellular dynamics during healing embryonic dermal wounds. In [12], Goto used mechano-chemical model, which is a simplified version of the full model $(1.1) - (1.3)$ mentioned above, for the formation of a somite. In order to build a powerful bio-mechanical model for describing biological problems difficult to solve, we refer the interested readers to this articles [13, 14, 15, 16]. The authors of these papers considered that the cell-sheet healing is largely a mechanical process where the chemical effect simply acts to increase the overall behavior. In [13] Lee et *all* have a biophysical description

of the collective migration of epithelial cells, they proposed a model that captures quantitatively cellular dynamics for wound healing and reproduced a complex cellular flow where results suggest that healing requires a mechanical process that is modified by the cell signaling, they stressed the important role of cellular exploration using a Maxwell viscoelastic model for healing of MDCK cell sheets and they carried out numerical tests in 1D and 2D. In [14], Vedula et *all* showed that the geometrical properties of the environment regulate the cell-migration by cell-interaction, in fact, using micro fabrication technique an epithelial cell-sheet can migrate into bands whose width varies from one to many cell diameters, they identified the collective migration patterns in response geometric constraints and observed the reduction of the strips width during each migration. In [15], Saez and his colleagues are studied the behavior of epithelial cells MDCK type on microfabricated supports designed to calculate the both interaction cell-cell and support-cell, they covered by a dense network of flexible micropillars whose deviation allows us to measure the traction forces which occur during cell healing, The authors showed experimentally using a deep study that the traction forces must be strong enough on the edge and becomes smaller by bringing the wound sheet center. In [16] Alexander J. Kabla realized a flexible framework for cell motility to study the requirement for the cell-coordination, he founded that cell-morality and mechanical interaction are sufficient to produce a variety of commonly observed behavior "in vitro" and "in vivo", also he noted that the migration sheet and sensitivity cells are examples of behavior emerging spontaneously from simple assumption, which could explain why the collective effect are omnipresent in nature.

2. Material and methods

2.1. Mathematical method

In what follows, the mechanical and chemical effects are neglected; only the biological effect is considered. Hence, the full coupled model $(1.1) - (1.3)$ reduces to the Fisher-KPP equation. Many scientific studies designed to investigate the validity of the Fisher-KPP equations. Fisher-KPP is a semilinear partial differential equation, introduced in 1937 by Fisher and Kolmogrov-Petrovski-Pisconoff [17, 18] which models the interaction between the speed and growth. To modelize the wounded cell sheet healing, we are disposed to implement numerically the 2D Fisher-KPP equation where the unknown n beiig the cell densitie.

$$n_t - D\Delta n + g(n) = 0, \quad (x, y) \in \Omega, \quad 0 < t \leq T, \tag{2.1}$$

with the initial condititon

$$n(x, y, 0) = n_0(x, y), \quad (x, y) \in \Omega, \tag{2.2}$$

and with the boundary conditions

$$n = 1, \quad \text{on} \quad \Gamma_D, \tag{2.3}$$

$$\frac{\partial n}{\partial y} = 0, \quad \text{on} \quad \Gamma_N, \tag{2.4}$$

where $g(n) = -rn(1 - n)$, Ω is a bounded rectangular open set of $\mathbb{R}^2$, Γ_D and Γ_N are respectively the vertical sides and the horizontal sides of Ω, see Figure 2 [19], D and r are a positive constants and stand for the cell diffusion coefficient and the cell proliferation rate respectively.

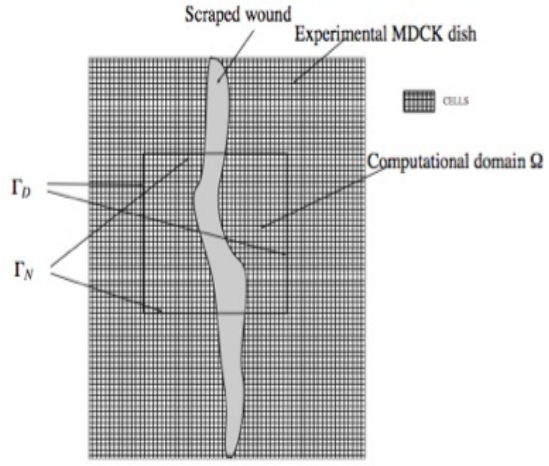

Figure 2. *A neighborhood Ω of the wound.*

2.2. Experimental method

The experimental method has been presented as following : we conducted five experiments for healing wound, which give five data sets, each composed of 360 images. From each set, we extract a series of 120 two-dimensional images of 1392×1040 pixels coded on 2 bytes, which corresponds to a step time of 6 minutes between two consecutive images. The tests are classified as follows :

• Assay I : considered as a control test or as a reference test (in which neither activator nor inhibitor migration was used).

• Assay II and Assay III : control test + HGF activator.

• Assay IV and Assay V : control test + inhibitor.

We recorded biological videos filming the various stages of wound closure. The videos were then segmented to obtain raw images, then they have been binarized to obtain images ready to deal with : the experimental density of cells, denoted n_{exp}, is provided. Using this density, we have successfully implemented experimental area of the wound :

$$W_{exp}(t) = \int_{\Omega} (1 - n_{exp}(x, y, t))dxdy. \tag{2.5}$$

These experimental results were compared to numerical results related to the numerical solution, denoted n_{num}, of the KPP-Fisher equation discretized in space using a finite difference scheme of order two and in time using the Crank Nicolson scheme with Splitting. It is more precisely to minimize with respect to parameters r and D the following two costs

$$J_U(r,\ D) = \int_{[T_0,T]} \int_{\Omega} |n_{num}(x, y, t) - n_{\text{exp}}(x, y, t)|dxdydt, \tag{2.6}$$

$$J_A(r,\ D) = \int_{[T_0,T]} |W_{num}(t) - W_{\exp}(t)|dt. \tag{2.7}$$

The first cost is the norm of the error between the numerical and experimental solution, while the second cost is the norm of the error between the numerical area and the experimental one. Figure (3) below shows the surfaces cost J_U and J_A in terms of parameters r and D.

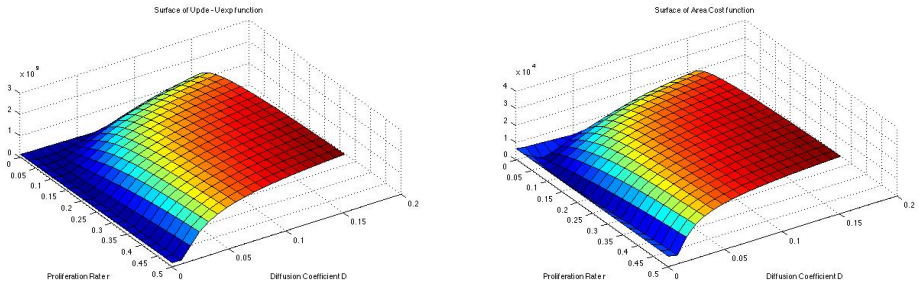

Figure 3. *Cost functions of surfaces J_U and J_A function of parameters (r,D)*

The numerical results on the wound area depending on time, obtained by Habbal et *al*, in the absence of activation and inhibition, published in [19], are shown in the following figures. The blue curve represents the experimental area variation of the wound with respect to time, while, the red curve represents the numerical area of the wound with respect to time.

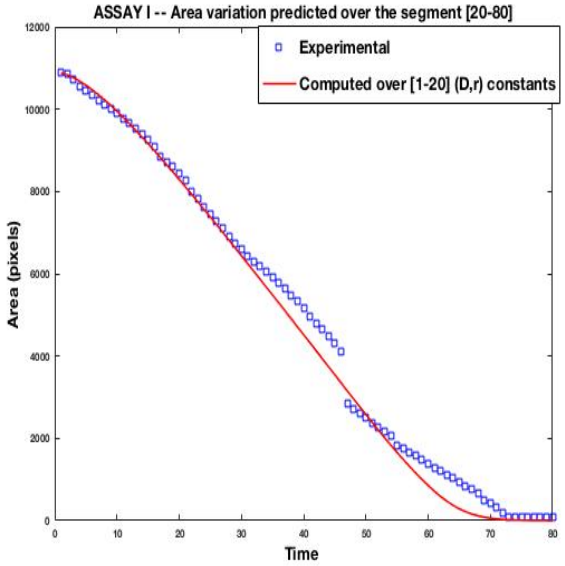

Figure 4. *The curves show the area of the wound depending on time for a reference sequence I.*

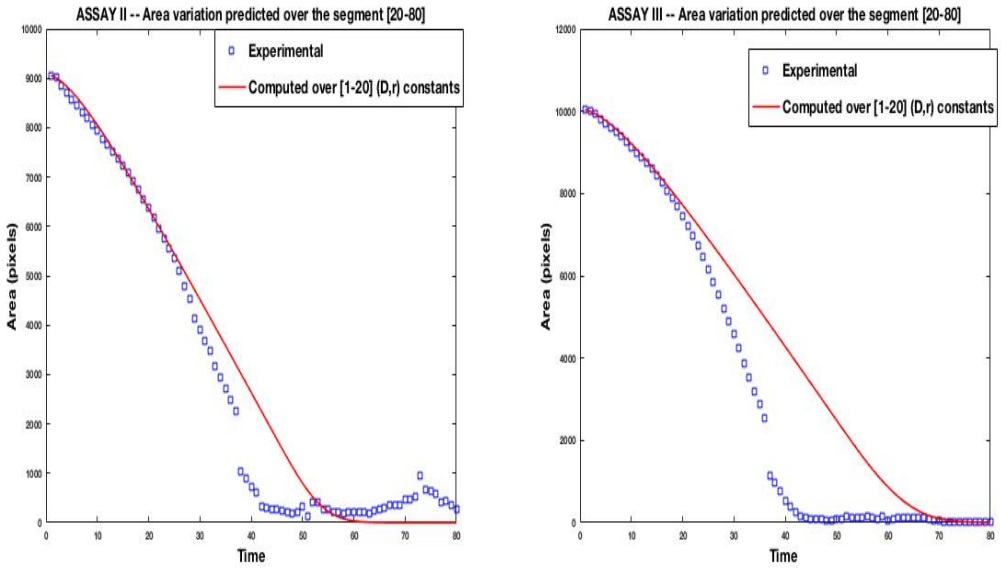

Figure 5. *The curves show the area of the wound depending on time for activated sequences II and III respectively.*

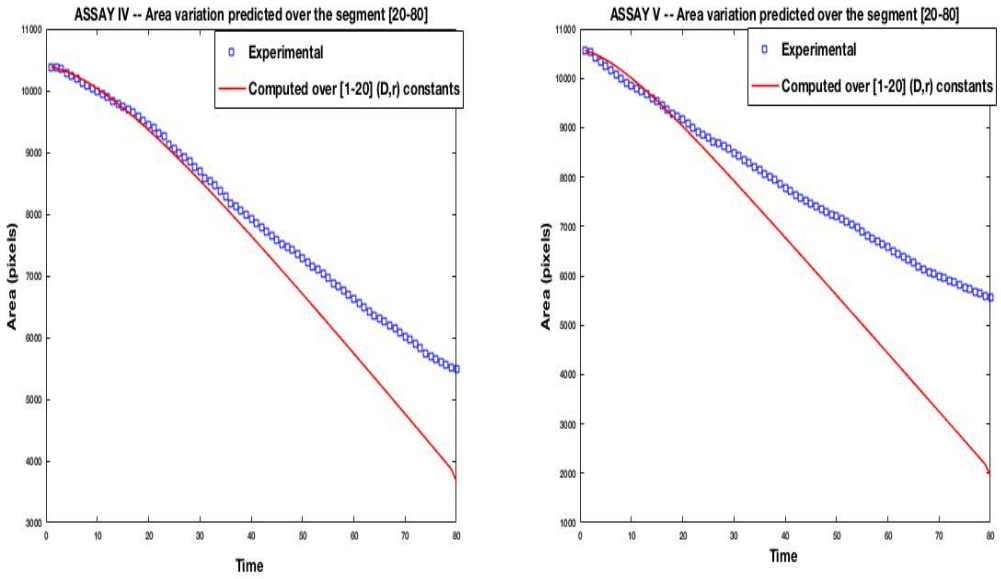

Figure 6. *The curves show the area of the wound depending on time for inhibited sequences IV and V respectively.*

For sequences with inhibited and activated condition migration, the above curves show that if the numerical area well approach the experimental area at the beginning of healing, this approximation is not at all satisfactory in the remaining time. To improve this approximation, we made recourse to activation and inhibition operations which are the novelty of this paper and the object of the following section.

From numerical point of view, activation and inhibition operations are taken into account by assuming that parameters D and r vary over time in a very precise manner. Charles Hansen suggested, after long studies on the choice of parameters including biological problems such as the prediction of cytotoxic drug interactions with DNA [20], a variation in sigmoid shape.

3. Results

3.1. Numerical Results

A sigmoid function, see [21, 22], is a S-shaped curve whose general expression is $\phi(t) = \frac{k}{1+\alpha exp(-\lambda t)}$. Its growth is slow at first, then accelerates strongly before slowing to end up not grow. In a first step, we have chosen to vary only parameter D over time :

$$D(t) = \frac{k}{1 + \alpha exp(-\lambda t)}, \qquad \lim_{t \to +\infty} D(t) = k$$

The numerical results are very satisfactory as shown in the following figures :

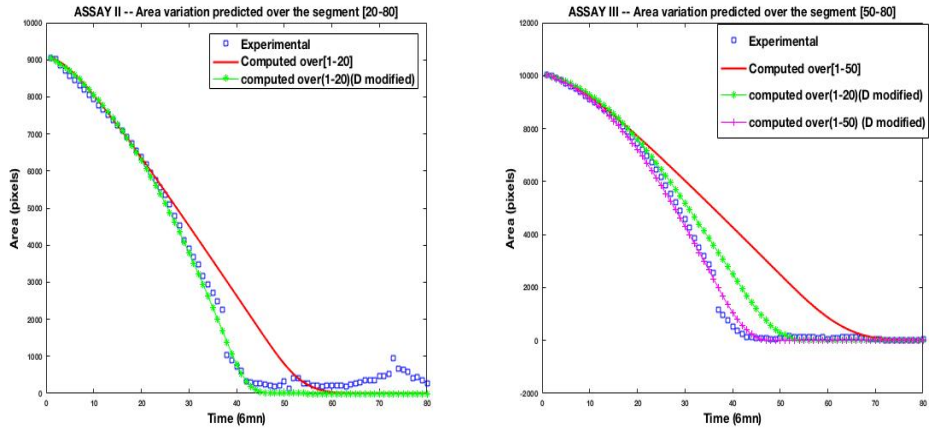

Figure 7. *The curves show the numerical areas obtained after activation with sequences II and III, respectively*

These numerical results with the optimal settings : $k^*_{II} = 2.00e-02$, $\lambda^*_{II} = 2.49e-02$, $\alpha^*_{II} = 3.00e+01$, $r^*_{II} = 2.26e-01$ for the second sequence and $k^*_{III} = 2.00e-02$, $\lambda^*_{III} = 4.00e-02$, $\alpha^*_{III} = 6.00e+01$, $r^*_{III} = 2.21e-01$ for the third sequence, realize the minimum of the error between the experimental and the numerical area. This optimi-

zation operation has been performed using the Matlab function "fmincon".

We are now interested in choosing a sigmoid pattern compatible with the inhibition operation to improve the numerical area for sequences IV and V.

$$D(t) = \frac{3k}{2} - \frac{k}{1 + \alpha exp(-\lambda t)}, \qquad \lim_{t \to +\infty} D(t) = \frac{k}{2}$$

Numerical results obtained are less satisfactory than those obtained in the case of activation as shown in Figure 8.

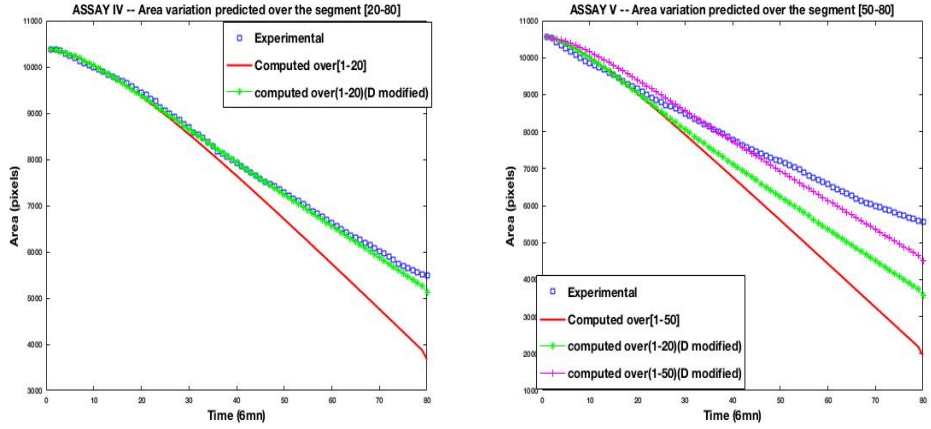

Figure 8. *The curves show the numerical areas obtained after inhibition with sequences IV and V respectively*
s

These numerical results, illustrated by the green curve, are obtained with the optimal settings : $k^*_{IV} = 1.32e-02$, $\lambda^*_{IV} = 4.00e-02$, $\alpha^*_{IV} = 3.00e+01$, $r^*_{IV} = 2.99e-02$ for the fourth sequence and $k^*_V = 2.00e-02$, $\lambda^*_V = 4.00e-02$, $\alpha^*_V = 3.00e+01$, $r^*_V = 2.93e-02$ for the fifth sequence. If the result obtained with inhibition and sequence IV is more or less acceptable, that of the sequence V is not at all acceptable. Hoping to get better results, we decided to also vary the parameter r over time.

Numerical results obtained become very satisfactory as shown in the following figures (Fig.9).

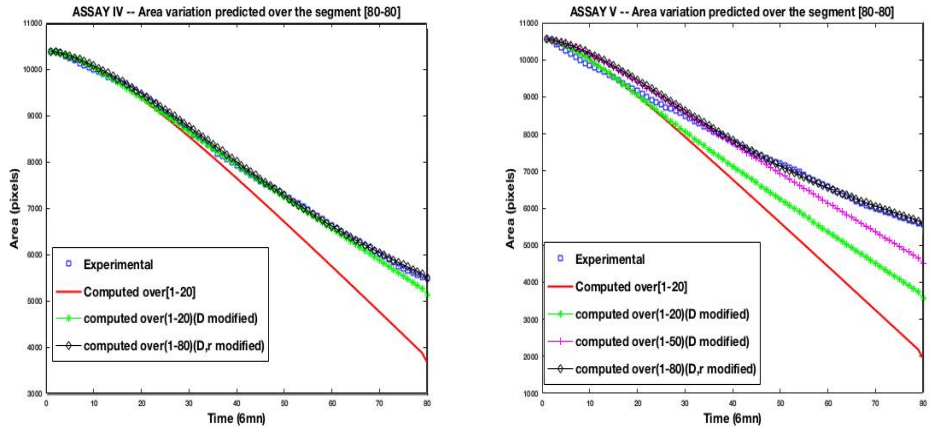

Figure 9. *The curves show the numerical areas obtained after inhibition with sequences IV and V respectively*

In both cases, the numerical curve (shown in black diamonds) coincides so much with the experimental curve (shown in continu blue line) that one can not see the latter. These numerical results are obtained with the optimal settings : $k^*_{DIV} = 2.00e-02$, $\lambda^*_{DIV} = 4.00e-02$, $\alpha^*_{DIV} = 3.4631e+03$, $k^*_{rIV} = 1.72e-02$, $\lambda^*_{rIV} = 1.00e-02$, $\alpha^*_{rIV} = 12.1045$ for the fourth sequence and $k^*_{DV} = 2.00e-02$, $\lambda^*_{DV} = 4.00e-02$, $\alpha^*_{DV} = 3.4631e+03$, $k^*_{rV} = 1.93e-02$, $\lambda^*_{rV} = 1.05e-02$, $\alpha^*_{rV} = 14.5041$ for the fifth sequence.

3.2. Theoretical Results

In this section, we are interested in estimating the error between the two curves presented in Figure 9 where the red curve shows the evolution of the wound area obtained by solving the 2D-Fisher-KPP equation with constant parameters and the black diamonds curve by choosing sigmoid patterns for parameters over time. For a similar study we refer to [23] and [24].

3.2.1. Diffusion and proliferation coefficients time-dependent

Consider the two following problems :

$$(P_1)\begin{cases} \partial_t u_1 = D\Delta u_1 + r u_1(1-u_1), & (x,y,t)\in\Omega\times(0,\ T], \quad (P_1.1)\\ u_1(x,y,0) = u_{1,0}(x,y), & (x,y)\in\overline{\Omega},\\ u_1(x,y,t) = u_H(x,y,t), & (x,y,t)\in\Gamma_D\times(0,\ T],\\ \frac{\partial u_1}{\partial n}(x,y,t) = g(x,y,t), & (x,y,t)\in\Gamma_N\times(0,\ T]. \end{cases}$$

$$(P_2)\begin{cases} \partial_t u_2 = D(t)\Delta u_2 + r(t) u_2(1-u_2), & (x,y,t)\in\Omega\times(0,\ T], \quad (P_2.1)\\ u_2(x,y,0) = u_{2,0}(x,y), & (x,y)\in\overline{\Omega},\\ u_2(x,y,t) = u_H(x,y,t), & (x,y,t)\in\Gamma_D\times(0,\ T],\\ \frac{\partial u_2}{\partial n}(x,y,t) = g(x,y,t), & (x,y,t)\in\Gamma_N\times(0,\ T]. \end{cases}$$

Lemme 3.1 *Suppose that* $u_{1,0}, u_{2,0} \in H^1(\Omega)$, $u_1 \in L^2(0,T;H^2(\Omega))$ *and* $u_2 \in L^2(0,T;H^1(\Omega))$, *then we have the following estimate :*

$$\|u_2 - u_1\|_{0,\Omega} \leq e^{L(t)}\|u_{2,0} - u_{1,0}\|_{0,\Omega} + e^{L(t)}\int_0^t e^{L(s)}\Big[|D(s) - D|\|\Delta u_1\|_{0,\Omega} + |\Omega||r(s)-r|\Big]ds. \quad (3.1)$$

The area of the wound at the instant t, defined by the formula (2.5), yields

$$\begin{aligned} |W_2(t) - W_1(t)| &\leq \int_\Omega |u_2 - u_1|dx \\ &\leq \sqrt{|\Omega|}\|u_2 - u_1\|_{0,\Omega}, \end{aligned}$$

where $|\Omega|$ *denotes the measure of* Ω.

Proof. Subtracting $(P_1.1)$ from $(P_2.1)$, we obtain the following equality

$$\partial_t(u_2 - u_1) = D(t)\Delta u_2 - D\Delta u_1 + r(t)u_2(1-u_2) - ru_1(1-u_1),$$

which give

$$\begin{aligned} \partial_t(u_2 - u_1) = &\ D(t)\Delta u_2 - D\Delta u_1 + r(t)u_2(1-u_2) - ru_1(1-u_1) \\ + &\ D(t)\Delta u_1 - D(t)\Delta u_1 + r(t)u_1 - r(t)u_1 + r(t)u_1^2 - r(t)u_1^2, \end{aligned}$$

consequently

$$\partial_t(u_2-u_1) = (D(t)-D)\Delta u_1 + D(t)\Delta(u_2-u_1) + r(t)(u_2-u_1)(1-(u_2+u_1)) + u_1(r(t)-r)(1-u_1).$$

Besides, using the scalar product of $L^2(\Omega)$ and multiplying scalarly by $u_2 - u_1$, it comes

$$\begin{aligned} (\partial_t(u_2-u_1),\ u_2-u_1) = &\ (D(t)-D)\underbrace{(\Delta u_1,\ u_2-u_1)}_{I1} + D(t)\underbrace{(\Delta(u_2-u_1),\ u_2-u_1)}_{I2} \\ + &\ r(t)\underbrace{((u_2-u_1)(1-(u_2+u_1)),\ u_2-u_1)}_{I3} + (r(t)-r)\underbrace{(u_1(1-u_1),\ u_2-u_1)}_{I4}. \end{aligned}$$

In the following, we will derive an estimate of each term $I1$, $I2$, $I3$ and $I4$ separately. To estime the first term $I1$, the Cauchy-Schwarz inequality leads to

$$|I1| \leq \|\Delta u_1\|_{0,\Omega}\|u_2 - u_1\|_{0,\Omega}. \quad (1)$$

With the help of Green's formula, the second term $I2$ can be written

$$\begin{aligned} I2 &= -\int_\Omega (\nabla(u_2-u_1),\ \nabla(u_2-u_1)) \\ &= -|u_2-u_1|^2_{1,\Omega}. \end{aligned} \quad (2)$$

The fact that $\|u_\alpha\|_{L(\Omega)} \leq 1,$ for $\alpha = 1, 2$, gives the following inequalities

$$|I3| \leq \|u_2 - u_1\|^2_{0,\Omega}, \quad (3)$$

$$|I4| \leq |\Omega| \|u_2 - u_1\|_{0,\Omega}. \tag{4}$$

The Poincaré inequality gives

$$-|u_2 - u_1|^2_{1,\Omega} \leq -\frac{1}{C^2(\Omega)} \|u_2 - u_1\|^2_{0,\Omega} \tag{5}$$

Gathering (1), (2), (3), (4) and (5) leads to the following result

$$\begin{aligned}(\partial_t(u_2 - u_1),\ u_2 - u_1) \leq\ & |D(t) - D| \|\Delta u_1\|_{0,\Omega} \|u_2 - u_1\|_{0,\Omega} - D(t)|u_2 - u_1|^2_{1,\Omega} \\ &+\ r(t)\|u_2 - u_1\|^2_{0,\Omega} + |\Omega||r(t) - r| \|u_2 - u_1\|_{0,\Omega},\end{aligned}$$

which implies that

$$\begin{aligned}\frac{d}{dt}\|u_2 - u_1\|^2_{0,\Omega} \leq\ & 2|D(t) - D| \|\Delta u_1\|_{0,\Omega} \|u_2 - u_1\|_{0,\Omega} - \frac{2D(t)}{C^2(\Omega)} \|u_2 - u_1\|^2_{0,\Omega} \\ &+\ 2r(t)\|u_2 - u_1\|^2_{0,\Omega} + 2|\Omega||r(t) - r| \|u_2 - u_1\|_{0,\Omega}.\end{aligned}$$

Inspired by the Gronwall's lemma [25] and putting $\|u_2 - u_1\|^2_{0,\Omega} = \phi(t)e^{2L(t)}$, we get

$$\begin{aligned}\phi'(t)e^{2L(t)} + 2L'(t)e^{2L(t)}\phi(t) \leq\ & 2|D(t) - D| \|\Delta u_1\|_{0,\Omega} \sqrt{\phi(t)e^{2L(t)}} \\ &+\ 2\phi(t)e^{2L(t)}\Big(r(t) - \frac{D(t)}{C^2(\Omega)}\Big) + 2|\Omega||r(t) - r|\sqrt{\phi(t)e^{2L(t)}}.\end{aligned}$$

By choosing $L'(t) = r(t) - \dfrac{D(t)}{C^2(\Omega)}$ which leads to $L(t) = \displaystyle\int_0^t \Big(r(s) - \frac{D(s)}{C^2(\Omega)}\Big)ds$ we get the following differential inequality

$$\phi'(t) \leq 2|D(t) - D| \|\Delta u_1\|_{0,\Omega} \sqrt{\phi(t)} e^{-L(t)} + 2|\Omega||r(t) - r| \sqrt{\phi(t)} e^{-L(t)}.$$

Let $\delta > 0$ and $t \in [0,\ T]$,

$$\frac{\phi'(t)}{2\sqrt{\phi(t) + \delta}} \leq \frac{\phi'(t)}{2\sqrt{\phi(t)}} \leq e^{-L(t)}\Big[|D(t) - D| \|\Delta u_1\|_{0,\Omega} + |\Omega||r(t) - r|\Big], \tag{6}$$

integrating the above inequality (6) over $(0, t)$, we have that

$$\int_0^t \frac{\phi'(s)}{2\sqrt{\phi(s) + \delta}} ds \leq \int_0^t e^{-L(s)}\Big[|D(s) - D| \|\Delta u_1\|_{0,\Omega} + |\Omega||r(s) - r|\Big] ds,$$

which gives

$$\sqrt{\phi(t) + \delta} - \sqrt{\phi(0) + \delta} \leq \int_0^t e^{-L(s)}\Big[|D(s) - D| \|\Delta u_1\|_{0,\Omega} + |\Omega||r(s) - r|\Big] ds,$$

passing to the limit, δ goes to 0, we obtain

$$\sqrt{\phi(t)} \leq \sqrt{\phi(0)} + \int_0^t e^{-L(s)}\Big[(D(s) - D)\|\Delta u_1\|_{0,\Omega} + |\Omega||r(s) - r|\Big] ds.$$

Finally, we get the desired estimate

$$\|u_2-u_1\|_{0,\Omega} \leq e^{L(t)}\|u_{2,0}-u_{1,0}\|_{0,\Omega}+e^{L(t)}\int_0^t e^{L(s)}\Big[|D(s)-D|\|\Delta u_1\|_{0,\Omega}+|\Omega||r(s)-r|\Big]ds.$$

The area of the wound at the instant t being defined by the formula (2.5). Hence the estimate of the area is given by :

$$\begin{aligned} |W_2(t)-W_1(t)| &\leq \int_\Omega |u_2-u_1|dx \\ &\leq \sqrt{|\Omega|}\|u_2-u_1\|_{0,\Omega} \end{aligned}$$

which completes the proof. ■

3.2.2. Estimate of $\|\Delta u_1\|_{0,\Omega}$

We are now seeking to estimate $\|\Delta u_1\|_{0,\Omega}$ as a function of the data $u_{1,0}$, D and r. In order to be reduced to a homogeneous problem, we make the following change of unknown : $w_1 = 1-u_1$ in the problem (P_1). The new unknown w_1 is then the solution to the following problem :

$$(P_3)\begin{cases} \frac{\partial w_1}{\partial t}(x,y,t) - D\Delta w_1(x,y,t) + rw_1(1-w_1) = 0, & (x,y,t)\in\Omega\times]0,T[, \\ w_1(x,y,0) = w_0(x,y) = 1-u_{1,0}, & (x,y)\in\overline{\Omega}, \\ w_1(x,y,t) = 0, & \text{on} \quad \Gamma_V\times[0,T], \\ \frac{\partial w_1}{\partial n}(x,y,t) = 0, & \text{on} \quad \Gamma_H\times[0,T]. \end{cases} \tag{7}$$

Lemme 3.2 *Suppose that $u_{1,0}\in H^1(\Omega)$ and $u_1\in L^2(0,T;H^2(\Omega))$, we get the following estimate*

$$\|\Delta u_1\|_{0,\Omega}^2 \leq 2\sum_{n=1}^{+\infty}\lambda_n^2\Big(\|1-u_{1,0}\|_{0,\Omega}^2 e^{-2D\lambda_n t} + r^2|\Omega|t\int_0^t e^{-2D\lambda_n(t-s)}ds\Big), \tag{8}$$

where $(\lambda_n)_{n\in\mathbb{N}^*}$ are eigenvalues of the following eigenvalue problem :

$$(P_4)\begin{cases} -\Delta v = \lambda v, & \textit{in} \quad \Omega, \\ v = 0, & \textit{on} \quad \Gamma_V, \\ \frac{\partial v}{\partial n} = 0, & \textit{on} \quad \Gamma_H. \end{cases} \tag{9}$$

Proof. We denote $(v_n)_{n\in N^*}$ the Hilbert basis of $V_0 = \{v\in H^1(\Omega) : v = 0 \quad \text{sur} \quad \Gamma_V\}$, formed of eigenvectors associated with eigenvalues $(\lambda_n)_{n\in N^*}$, such that each pair (v_n,λ_n) is the solution of eigenvalue problem (P_4). It is well known that the sequence of eigenvalues $(\lambda_n)_{n\in N^*}$ is strictly positive, increasing and tends towards the infinity when n tends to the infinity. Moreover, the basis $(v_n)_{n\in N^*}$ is orthonormal in $L^2(\Omega)$ [24].
Since the problem (P_3) satisfies the same boundary conditions as the problem (P_4), we look for its solution in the form :

$$w_1(x,t) = \sum_{n=1}^{+\infty}\alpha_n(t)v_n(x).$$

After calculations, details of which are found for example in [24], we get

$$w_1(x,t) = \sum_{n=1}^{+\infty} \Big((w_0, v_n)_{0,\Omega} e^{-D\lambda_n t} - r \int_0^t (w_1(1-w_1), v_n)_{0,\Omega} e^{-D\lambda_n (t-s)} ds \Big) v_n(x),$$

which give

$$\Delta w_1 = -\sum_{n=1}^{+\infty} \lambda_n \Big((w_0, v_n)_{0,\Omega} e^{-D\lambda_n t} - r \int_0^t (w_1(1-w_1), v_n)_{0,\Omega} e^{-D\lambda_n (t-s)} ds \Big) \Delta v_n(x),$$

consequently

$$\|\Delta u_1\|^2_{0,\Omega} = \sum_{n=1}^{+\infty} \lambda_n^2 \Big((1-u_{1,0}, v_n)_{0,\Omega} e^{-D\lambda_n t} - r \int_0^t (u_{1,0}(1-u_1), v_n)_{0,\Omega} e^{-D\lambda_n (t-s)} ds \Big)^2. \tag{10}$$

Using the following inequalities

$$(u_1(1-u_1), v_n)^2_{0,\Omega} \leq \|u_1(1-u_1)\|^2_{0,\Omega} \|v_n\|^2_{0,\Omega} \leq |\Omega|,$$

$$\Big(r \int_0^t (u_1(1-u_1), v_n)_{0,\Omega} e^{-D\lambda_n (t-s)} ds \Big)^2 \leq r^2 |\Omega| t \int_0^t e^{-2D\lambda_n (t-s)} ds,$$

the expression (10) becomes

$$\|\Delta u_1\|^2_{0,\Omega} \leq 2 \sum_{n=1}^{+\infty} \lambda_n^2 \Big(\|1-u_{1,0}\|^2_{0,\Omega} e^{-2D\lambda_n t} + r^2 |\Omega| t \int_0^t e^{-2D\lambda_n (t-s)} ds \Big).$$

3.2.3. Diffusion coefficient D depending on time

In this section, we are interested in estimating the error between the green curve and the red one presented in Figure 7 and Figure 8. Therefore, we consider the following problem

$$(P_5) \begin{cases} \partial_t u_5 = D(t)\Delta u_5 + r u_5(1-u_5), & (x,\ t) \in \Omega \times (0,\ T], \quad (P_5.1) \\ u_5(x,0) = u_{5,0}(x), & x \in \overline{\Omega}, \\ u_5(x,\ t) = u_H(x,\ t), & (x,\ t) \in \Gamma_D \times (0,\ T], \\ \frac{\partial u_5}{\partial n}(x,\ t) = g(x,\ t), & (x,\ t) \in \Gamma_N \times (0,\ T]. \end{cases}$$

Lemme 3.3 *Suppose that $u_{1,0}, u_{5,0} \in H^1(\Omega)$, $u_1 \in L^2(0,T; H^2(\Omega))$ and $u_5 \in L^2(0,T; H^1(\Omega))$, then we have the following estimate :*

$$\|u_5 - u_1\|_{0,\Omega} \leq e^{L(t)} \|u_{5,0} - u_{1,0}\|_{0,\Omega} + e^{L(t)} \int_0^t e^{L(s)} [|D(s) - D| \|\Delta u_1\|_{0,\Omega} e^{-L(s)}$$

Hence the estimate of the area is given by :

$$\begin{aligned} |W_5(t) - W_1(t)| &\leq \int_\Omega |u_5 - u_1| dx \\ &\leq \sqrt{|\Omega|} \|u_5 - u_1\|_{0,\Omega} \end{aligned}$$

Proof. In an analogous manner to the proof of Lemma 3.1, we can demonstrate this result.

4. Conclusions and perspectives

In order to model cellular dynamics, a simple model of Fisher-KPP type, considering only the biological effect, was considered in the first step. The comparison of numerical results obtained, in the case where the proliferation and diffusion parameters are constant, with experimental results shows the insufficiency of Fisher-KPP model to accurately represent the activated and inhibited dynamics. Nevertheless, the activation and inhibition operations (D and r time-dependent) provide more effective results, which is coherent with the two estimations (3.1) and (3.2).

In order to better model the cellular dynamics, a coupled model is suggested. It consists at the Fisher-KPP equation coupled with the mechanics equation ; the behavior being purely elastic. Moreover, the numerical implementation of such coupled model is in progress.

5. Bibliographie

[1] MURRAY J.D., « Mathematical Biology : I. An Introduction, Third Edition », *Springer,Interdisciplinary Applied Mathematics*, vol. 17, 2001.

[2] MURRAY J.D. , « Mathematical Biology : II. Spatial Models and Biomedical Applications », *Springer,Interdisciplinary Applied Mathematics*, vol. 18, 2011.

[3] PAGE KAREN M., MAINI PHILIP K., A.M. MONK. NICHOLAS, « Complex pattern formation in reaction-diffusion systems with spatially varying parameters », *Physica*, vol. 202, n° , 2005.

[4] OLSEN L., MAINI P.K., SHERRATT J.A., « Spatially Varying Equilibria of Mechanical Models : Application to Dermal Wound Contraction », *Mathematical Bisciences*,vol. 147, n° 113, 1998.

[5] FENTEANY G., JANMEY P. A., STOSSEL T. P., « Signaling pathways and cell mechanics involved in wound closure by epithelia cell sheets », *Current Biology*, vol. 10, n° 831, 2000.

[6] BAO QI., HUGHES R.C., « Galectin-3 and polarized growth within collagen gels of wild-type and ricin-resistant mdck renal epithelial cells », *Glycobiology*, vol. 9, n° 5, 1999.

[7] QINGHUI MENG, JAMES M. MASON, DEBRA PORTI, ITZHAK D. GOLDBERG, ELIOT M. ROSEN, SAIJUN FAN, « Hepatocyte growth factor decreases sensitivity to chemotherapeutic agents and stimulates cell adhesion, invasion, and migration », *Biochem. Biophys. Res. Commun.*, vol. 274, n° 772, 2000.

[8] OLSEN L., MAINI P.K., SHERRATT J.A., « A mechanochemical model for normal and abnormal dermal wound repair », *Nonlinear Analysis, Theory, Methods & Applications*, vol. 30, n° 6, 1997.

[9] OLSEN L., MAINI P.K., SHERRATT J.A., « A Mechanochemical Model for Adult Dermal Wound Contraction and the Permanence of the Contracted Tissue Displacement Profile », *J. theor. Biol.*, vol. 177, 1995.

[10] PERELSON A. S., MAINI P. K., MURRAY J. D., HYMAN J. M. , OSTER G. F.G. F., « Nonlinear pattern selection in a mechanical model for morphogenesis », *Journal of Mathematical biology. Springer Veriag*, vol. 24, n° 525, 1986.

[11] SHERRATT J. A., « Actin aggregation and embryonic epidermal wound healing », *Journal of Mathematical biology. Springer Veriag*, vol. 31, n° 703, 1993.

[12] GOTO Y., « A 2-dimensional mechanical model of the formation of a somite », *International journal of numerical analysis and modeling*, vol. 10, n° 1, 2013.

[13] LEE P., WOLGEMUTH C. W., « Crawling Cells Can Close Wounds without Purse Strings or Signaling », *PLoS Computational Biology*, vol. 7, 2011.

[14] VEDULA S. R. K., LEONG M. C., LAI T. L. , HERSEN P., KABLA A. J., LIM C.T., LADOUX B., « Emerging modes of collective cell migration induced by geometrical constraints », *PNAS*, vol. 109, 2012.

[15] SAEZ A., ANON E., GHIBAUDO M., O DU ROURE, MEGLIO J-M DI., HERSEN P., SILBERZAN P., BUGUIN A., LADOUX B., « Traction forces exerted by epithelial cell sheets », *J. Phys. : Condens. Matter*, vol. 22, n° 9, 2010.

[16] KABLA A. J., « Collective cell migration : leadership, invasion and segregation », *J. R. Soc. Interface*, vol. 9, 2012.

[17] FISHER R., « The wave of advance of avantageous genes », *Annais of Eugenics*, vol. 7(4), 355-369, 1937.

[18] KOLMOGOROV A., PETROVSKY I., PISKUNOV N.,« A study of the equation of diffusion with increase in the quantity of matter, and its application to a biological problem », *Byul. Moskovskogo Gos.Univ.*, vol. 1(6), 1-25, 1937.

[19] HABBAL A., BARELLI H., MALANDAIN G., « Assessing the ability of the 2D Fisher-KPP equation to model cell-sheet would clousure », *Mathematical Biosciences*, vol. 252, n° 45, 2014.

[20] HANSEN C. M. , « Polymer science applied to biological problems : prediction to cytotoxic drug interactions with DNA », *European Polymer Journal*, vol. 44, 2008.

[21] HAMEL É. , « Modélisation mathématique de la déxpression synaptique et des périodes réfractaires pour le quantron », 2013.

[22] YEGANEFAR N., « Définitions et analyse de stabilité pour les systèmes à retard non linéaires », Novembre 2006.

[23] BREZIS H., « Analyse fonctionnelle : Théorie et applications », *Dunod*, 1999.

[24] RAVIART P.A., THOMAS J.M., « Introduction à l'analyse numérique des équations aux dérivées partielles », *Masson*, 1983.

[25] CLARK D. S. , « Short proof of a discrete Gronwall inequality », *Discrete Applied Mathematics*, vol. 16, 279-281, 1987.